Journal of Alloys and Compounds 509 (2011) 872–877

Contents lists available at ScienceDirect

Journal of Alloys and Compounds

journal homepage: www.elsevier.com/locate/jallcom

Effects of annealing conditions on the properties of TiO_2/ITO-based photoanode and the photovoltaic performance of dye-sensitized solar cells

Chih-Ming Chen*, Yu-Chun Hsu, Sheng-Jye Cherng

Department of Chemical Engineering, National Chung Hsing University, Taichung 402, Taiwan

ARTICLE INFO

Article history:
Received 30 June 2010
Received in revised form
18 September 2010
Accepted 22 September 2010
Available online 1 October 2010

Keywords:
Electrode materials
Semiconductors
Photoconductivity and photovoltaics
Annealing

ABSTRACT

Photovoltaic performance of dye-sensitized solar cell (DSSC) is enhanced by a two-step annealing process of the photoanode. The 1st-step of annealing is performed in oxygen at 450 °C for 30 min which effectively removes the residual organics originated from the TiO_2 precursor pastes. This enhances the dye adsorption on the TiO_2 nanoparticles and raises the short-circuit current density (J_{SC}). The 2nd-step of annealing is performed in nitrogen at 450 °C for 10 min which removes extra oxygen atoms resulted from the incorporation of oxygen atoms into the tin-doped indium oxide (ITO) film during the 1st-step of annealing. This reduces the sheet resistance of ITO and thereby enhances the fill factor (FF). With the enhanced J_{SC} of 15.9mAcm^{-2} and FF of 0.65, the AM1.5 solar to electric conversion efficiency (η) of DSSC reaches 6.7% which is better than that based on the conventional one-step air annealing (η = 5.53%, J_{SC} = 14.08 mA cm^{-2}, FF = 0.6).

1. Introduction

Transparent conductive oxides (TCOs) have been widely used in the optoelectronic devices due to superior light transmittance and electrical conductivity. For example, dye-sensitized solar cell (DSSC) uses TCO-coated glass as the electrode substrate. Tin-doped indium oxide (ITO) is one of the TCOs that are most frequently used in DSSCs [1–3]. A typical DSSC is composed of three components: a dye-adsorption TiO_2 photoanode, a Pt-coated counterelectrode, and an electrolyte containing iodide–triiodide redox couple. The photoanode is fabricated by coating a nanocrystalline TiO_2 film on an ITO-coated glass substrate, followed by dye adsorption on the TiO_2 nanoparticles. Prior to dye adsorption, the TiO_2 film must be annealed at about 450 °C for around 30 min. This annealing/sintering process can enhance the interconnection of the TiO_2 nanoparticles and also enhance the adhesion between the TiO_2 nanoparticles and the ITO film. In addition, the annealing process is generally conducted in air. This is because it is generally believed that the residual organics originated from the TiO_2 colloidal pastes can be removed in an oxygen-containing atmosphere [4]. Removal of the residual organics can enhance adsorption of dye molecules onto the TiO_2 nanoparticles.

Though a structurally and electrically excellent TiO_2 film can be obtained after air annealing, the electrical resistivity of the ITO film increases [3–5]. The increase of resistivity is attributed to the decrease of oxygen vacancies in the ITO film [4,6,7]. During annealing, the oxygen atoms in the air diffuse into the ITO film and occupy the oxygen vacancies. Because an oxygen vacancy can provide a pair of free electrons, the decrease of oxygen vacancies simultaneously results in the decrease of free electrons, and thus the resistivity of the ITO film increases. The increase of ITO resistivity due to its thermal instability significantly degrades the photovoltaic performance of DSSCs.

To avoid the detrimental effects caused by the thermal instability of ITO, highly heat-resistive fluorine-doped tin oxide (FTO) was introduced in the DSSC application [2]. However, the sheet resistance (R_S) of FTO is higher than that of as-deposited ITO because the solubility of fluorine in SnO_2 is much less than that of tin in In_2O_3 [3]. The optical properties of FTO are also not as good as those of ITO [3]. Furthermore, the commercial cost of FTO is higher than that of ITO; this will unavoidably raise the cell cost when ITO was replaced by FTO. Therefore, based on the above viewpoints, ITO is still a good TCO for the DSSC application as long as its thermal stability can be substantially improved.

An effective method of improving the thermal stability of ITO was to deposit a thin layer of metal oxides, such as SnO_2, on the ITO to form a double-layered TCO [3]. The SnO_2 layer functioned as a passivation/barrier layer which separated the ITO from air, and thus the loss of oxygen vacancies during annealing could be retarded. However, the thickness of the SnO_2 layer must be carefully controlled because thicker SnO_2 decreases the light transmittance but thinner SnO_2 degrades the barrier effect.

In this present study, we demonstrated that the thermal stability of ITO could also be improved by simply adjusting the annealing

* Corresponding author. Tel.: +886 4 22859458; fax: +886 4 22854734.
E-mail address: chencm@nchu.edu.tw (C.-M. Chen).

0925-8388/$ – see front matter © 2010 Elsevier B.V. All rights reserved.
doi:10.1016/j.jallcom.2010.09.118

Table 1
Details of four types of annealing conditions and sheet resistances and energy gaps of the ITO substrates before and after annealing treatments.

Annealing type	Annealing conditions						Sheet resistance of ITO ($\Omega\square^{-1}$)	E_g (eV)
	1st-step			2nd-step				
	Before annealing						4.6–5.18	4.043
1st	Air	450 °C	30 min				24.15–25.88	3.943
2nd	Air	450 °C	30 min	N_2	300 °C	10 min	16.10–17.83	3.969
						60 min	13.80–15.53	3.974
					450 °C	10 min	8.63–9.78	3.995
						60 min	7.48–9.78	4.011
3rd	O_2	450 °C	30 min				29.9–32.2	3.934
4th	O_2	450 °C	30 min	N_2	300 °C	10 min	21.28–22.43	3.943
						60 min	17.25–18.4	3.957
					450 °C	10 min	9.78–10.35	3.997
						60 min	8.63–9.78	3.994

conditions. In addition, it was found that the annealing atmosphere had a significant effect on the removal of residual organics from the TiO_2 film. This present study systematically investigated the effects of annealing conditions on the performance of photoanodes, including the electrical and optical properties of ITO and the removal of residual organics from TiO_2. The photovoltaic performance of DSSCs was enhanced by employing a two-step O_2/N_2 annealing process of the photoanodes.

2. Experimental procedures

2.1. Annealing treatments of the ITO glass substrates in different atmospheres

Commercial ITO-coated glass sheets (Gem Technology Optoelectronics, Taiwan) were used as the substrates. The thicknesses of the glass and ITO film are 1.1 mm and 200 nm, respectively. The glass substrates were cut into lots of pieces with a dimension of 15 mm × 20 mm. The glass pieces were ultrasonically cleaned in lotion used for cleaning ITO glass, ethanol, and deionized water, and then dried up in a 40 °C oven. Four types of annealing treatments of the ITO glass substrates were performed. For the 1st type of annealing treatment, the ITO glass substrates were placed in a furnace at 450 °C for 30 min as a conventional annealing process for the photoanode of DSSC. No specific atmosphere was set for this annealing tretment, it was performend only in air. For the 2nd type, the ITO glass substrates underwent the above-mentioned air annealing were subsequently annealed in nitrogen (99.996% purity) at 300 and 450 °C for 10–60 min. The 3rd type of annealing process was only performed in oxygen (99.996% purity) at 450 °C for 30 min. The oxygen-annealed ITO glass substrates were subsequently re-annealed in nitrogen at 300 and 450 °C for 10–60 min as the 4th type of annealing treatment. Table 1 summarized the details of the above four types of annealing conditions. Overall, the 1st and 3rd types of annealing were one-step process while the 2nd and 4th types of annealing were two-step process.

2.2. Characterization of the ITO glass substrates after various annealing treatments

After the annealing treatments mentioned above, the sheet resistances of the ITO films were measured using a four-point probe. The light transmittance of the annealed ITO glass substrate in a wavelength ranging from 300 to 800 nm was measured using a UV–vis spectrometer. Identification of the crystal structures of the ITO films was carried out using an X-ray diffractometer (XRD). The surface compositions of the ITO films were determined using an X-ray photoelectron spectrometer (XPS).

2.3. Preparation of TiO_2-coated ITO glass substrate as photoanode for DSSC

The photoanode of DSSC was fabricated by screen printing a mesoporous TiO_2 film with a thickness of about 15 μm onto the ITO glass substrates. The material used for screen printing was a commercial TiO_2 paste (Tripod Technology, Taiwan). The printed area of the TiO_2 film was 0.283 cm^2. After screen printing, four types of annealing treatments listed in Table 1 were performed on the TiO_2-coated ITO substrates. Based on the four types of annealing treatments, four different types of photoanodes were prepared for DSSC assembly.

2.4. DSSC assembly and analysis of photovoltaic performance

The as-annealed photoanodes were immersed in an ethanol solution of N719 dye (0.4 mM) for 12 h. After dye adsorption, the photoanode was assembled with the counterelectrode made of another ITO glass substrate coated with a sputtered platinum layer (~100 nm thick). A 25-μm-thick hot-melt film (SX-1170-25, Solaronix) was used as the spacer. A liquid electrolyte (0.2 M PMII (3-propyl-1-methylimidazolium iodide), 0.1 M LiI, 0.05 M iodine, 0.5 M TBP (4-tert-butylpyridine), and 0.2 M TBAI (Tetrabutylammoniumiodide) in AN (Acetonitrile) and VN (Valeronitrile) (volumetric ratio = 85:15)) was injected into the cell to fill the gap between the two electrodes. Cell performance was evaluated under AM1.5 (1 sun) illumination with a solar simulator (YSS-E40, Yamashita Denso, Japan). Photocurrent–voltage (*J–V*) curves were recorded using a computer-controlled digital source meter (Keithley, model 2400).

3. Results and discussion

3.1. Sheet resistances of the ITO substrates after various annealing treatments

Table 1 lists the sheet resistances of the ITO glass substrates before and after annealing treatments. The sheet resistance increased to 24.15–25.88 $\Omega\square^{-1}$ after annealing in air (1st type of annealing), which was about 5 times larger than that before annealing (4.6–5.18 $\Omega\square^{-1}$). The carrier concentration of the ITO is contributed by both oxygen vacancies and substitutional tin dopants created during film deposition. The increase of sheet resistance was principally attributed to the loss of oxygen vacancies because the annealing was performed in an oxygen-containing atmosphere. In other words, oxygen atoms would diffuse into the ITO film and occupy the oxygen vacancies during annealing, reducing the carrier concentration and thus increasing the sheet resistance. The increase of sheet resistance was more significant (29.9–32.2 $\Omega\square^{-1}$) when the ITO substrate was annealed in oxygen (3rd type of annealing). This confirmed that oxygen was the cause of the increase of the ITO sheet resistance. However, when the above two ITO substrates were further annealed in nitrogen (2nd and 4th types of annealing), the sheet resistances dramatically reduced. We tried two different annealing temperatures (300 °C and 450 °C) and found that higher annealing temperature was more beneficial for the reduction of sheet resistance. We also tried two different annealing times (10 min and 60 min), and the results revealed that the sheet resistances decreased with increasing the annealing time.

The reduction of sheet resistance indicated that the oxygen vacancies in the ITO film increased after annealing in nitrogen. In other words, the oxygen concentration reduced. Table 2 shows the surface compositions of the ITO films before and after 3rd and 4th types of annealing treatments. Obviously, the oxygen concentration increased when the ITO substrate was annealed in oxygen (3rd type of annealing), resulting in raised sheet resistance as shown in Table 1. After further annealing in nitrogen (4th type of annealing), the oxygen concentration decreased. Therefore, the sheet resistance of ITO reduced. It was suggested that a concentration gradient of oxygen generated from the inner of ITO to the outer nitrogen (oxygen-free) atmosphere, which provided a driving force for out-diffusion of oxygen atoms. As a

Table 2
Surface compositions of the ITO films before and after 3rd and 4th types of annealing treatments (obtained from XPS data).

Annealing type	Annealing conditions						Chemical composition in at.%			
	1st-step			2nd-step			O	In	Sn	C
	Before annealing						54.7	36.0	2.9	6.2
3rd	O_2	450 °C	30 min				66.0	27.7	2.6	3.7
4th	O_2	450 °C	30 min	N_2	450 °C	10 min	57.9	35.4	2.7	4.0
						60 min	57.6	36.9	2.7	2.9

result, the oxygen vacancy increased and thus the sheet resistance reduced.

3.2. Optical transmittance of the ITO substrates after various annealing treatments

Fig. 1 shows the optical transmittance spectra of the ITO substrates before and after various annealing treatment. The average transmittance in the visible region of annealed ITO substrates was approximately higher than 80%, indicating that the annealing treatment used in the present study had no harmful effects on the ITO transmittance. Fig. 1(b) and (d) are magnifications of the spectra in the ultraviolet region in Fig. 1(a) and 1(c), respectively. It was found that the absorption edges of the spectra shifted to the long wavelength region, which is called red shift, after annealing in air (1st type) and oxygen (3rd type). However, blue shift of the absorption edges, that is, the absorption edges shifted to the short wavelength region, was observed when the ITO substrates were further annealed in nitrogen (2nd and 4th types). This phenomenon can be explained by Burstein–Moss (BM) effect [8–10]. According to Burstein–Moss effect, the bandgap energy of the ITO substrate is expressed as

$$E_g = E_{g0} + \Delta E_g^{BM} \tag{1}$$

where E_g and E_{g0} are the bandgap energy and the intrinsic bandgap energy as carrier density is zero, respectively. ΔE_g^{BM} is the bandgap energy broadening due to BM effect and can be expressed as

$$\Delta E_g^{BM} = \frac{h^2}{8m*}\left(\frac{3}{\pi}\right)^{2/3} n_e^{2/3} \tag{2}$$

where h is Planck's constant, m^* is the reduced effective mass of the electron carriers, and n_e is carrier concentration. It is clear that when the carrier concentration, n_e, increases, ΔE_g^{BM} increases, and so is E_g. This means that more energy is needed for the carriers in the valence band jumping to the unfilled conduction band. Therefore, the absorption edge shifts to the short wavelength (high energy) region. In other words, when the carrier concentration decreases, the absorption edge will shift to the long wavelength (low energy) region. Based on above statements, the variation of the absorption edges shown in Fig. 1(b) and (d) can be used to judge the variation of the carrier concentrations in the ITO films. For the ITO substrates annealed in air and oxygen, the absorption edges shifted to the long wavelength region, indicating that the carrier concentration decreased and the sheet resistance increased, which was in good agreement with the data of Table 1. However, the absorption edges turned to the short wavelength region after further annealing in nitrogen. This revealed that further nitrogen annealing could enhance the carrier concentration and thereby reduce the sheet resistance, which was also consistent with the data of Table 1.

The bandgap energy (E_g) can be obtained by the following two equations:

$$T = (1-R)^2 e^{-\alpha d} \tag{3}$$

$$\alpha h\nu = A(h\nu - E_g)^{1/2} \tag{4}$$

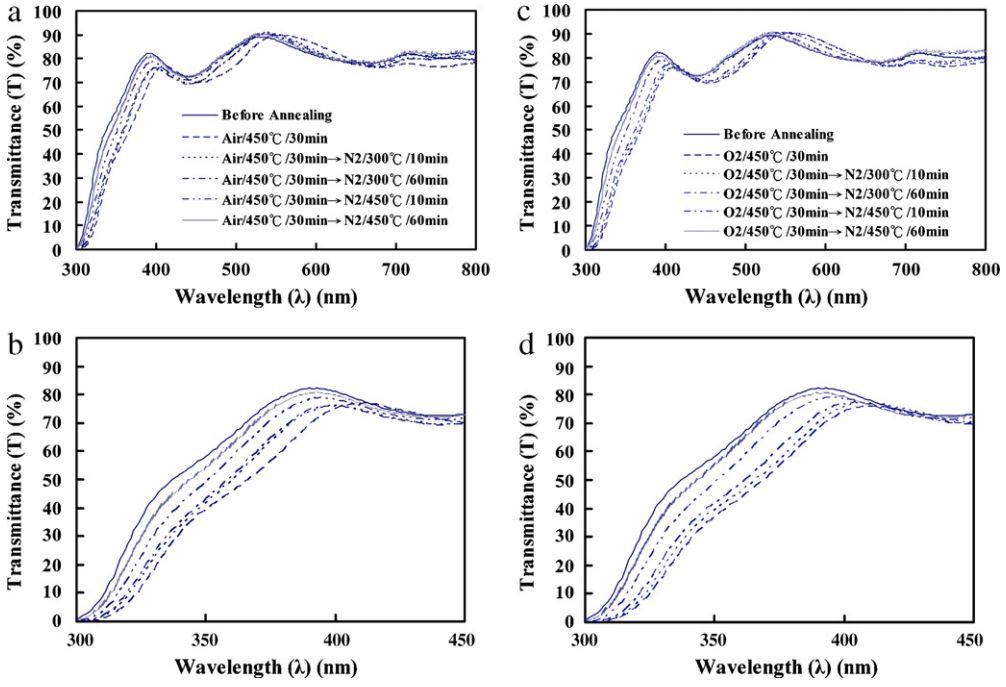

Fig. 1. Optical transmittance spectra of the ITO substrates before and after various annealing treatments. (a) The 1st and 2nd types of annealing, (b) a magnification of the spectra in the ultraviolet region of (a), (c) the 3rd and 4th types of annealing, (d) a magnification of the spectra in the ultraviolet region of (c).

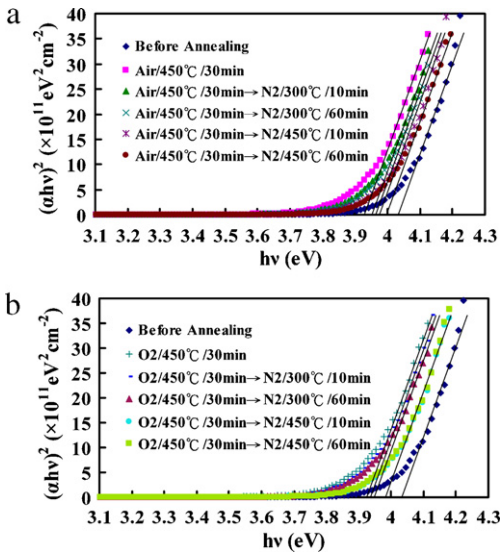

Fig. 2. Dependence of photon energy ($h\nu$) on $(\alpha h\nu)^2$ for the ITO films before and after annealing. (a) the 1st and 2nd types of annealing, (b) the 3rd and 4th types of annealing.

where T is the transmittance, R the reflectance, d the thickness of the ITO film, α the light absorption coefficient, A a constant, and $h\nu$ the photon energy. By plotting $(\alpha h\nu)^2$ versus $h\nu$ for the ITO films before and after annealing, as shown in Fig. 2, E_g can be determined by extrapolations of the linear regions of the plots to zero absorption ($\alpha h\nu = 0$). The values of E_g for various annealing treatments were listed in Table 1. The E_g decreased as the sheet resistance of the ITO films increased, i.e. the carrier concentration in the ITO films reduced.

3.3. Crystallinity of the ITO substrates after various annealing treatments

XRD patterns of the ITO substrates after various annealing treatment are shown in Fig. 3. The ITO substrates before annealing exhibited an amorphous structure with defects and non-stoichiometric compositions like In_2O_{3-x} and SnO_{2-x}. After annealing in air, the crystallinity of the ITO films became better and the preferential crystalline planes of the In_2O_3 crystal included (6 2 2), (4 4 0), (4 0 0), and (2 2 2). In general, annealing in oxygen-containing atmosphere (e.g. air) can improve the crystallinity of the ITO films because the oxygen vacancies can be eliminated by incorporation of oxygen atoms into the ITO films, leading to stoichiometric compositions like In_2O_3. Annealing can also remove defects like dislocations and grain boundaries, and thus improve the crystallinity. However, successive annealing in nitrogen made the crystallinity of the ITO films worse with increasing the annealing temperature and time. As discussed in Section 3.1, annealing in nitrogen would enhance out-diffusion of oxygen atoms from the ITO films. Therefore, the oxygen vacancies in the ITO films increased which degrade the crystallinity.

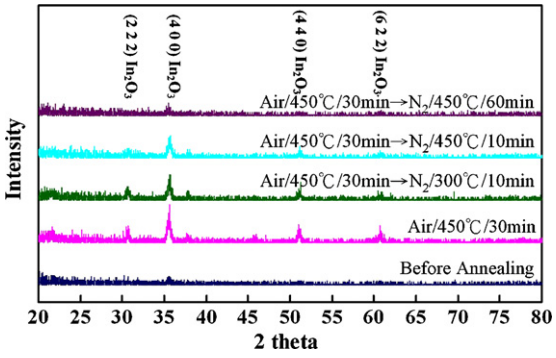

Fig. 3. XRD patterns of the ITO substrates before and after various annealing treatment.

3.4. Photovoltaic performance of DSSCs assembled with various annealed photoanodes

Table 3 lists the photovoltaic performance of DSSCs assembled with various annealed photoanodes. It was found that annealing conditions had significant effects on the cell performance. The DSSC assembled with the conventional photoanode (treated with 1st type of annealing) exhibited efficiency (η) of 5.53%. When the DSSCs were assembled with the photoanodes underwent 2nd type of annealing, enhanced cell efficiencies were observed. As discussed in Table 1, the additional 2nd-step annealing in nitrogen can reduce the raised sheet resistance of ITO caused by the 1st-step air annealing. The internal resistance of DSSC reduced accordingly and thus the fill factor (FF) was improved as shown in Table 3. The 2nd-step annealing in nitrogen also enhanced the short-circuit current density (J_{SC}). Therefore, the cell efficiency was enhanced.

For the 3rd type of annealing, the resultant DSSC exhibited efficiency of 5.84%. Its fill factor was lower than that based on the 1st type of annealing, which could be attributed to the fact that the sheet resistance of the ITO greatly increased after annealing in oxygen (Table 1). However, due to the increase in J_{SC}, the efficiency of this type of DSSC was still comparable to that of the DSSC based on the 1st type of annealing. Conventionally, annealing treatment of the photoanodes was performed in oxygen-containing atmosphere (e.g. air) in order to remove the residual organics originated from the TiO_2 precursor pastes [4]. Since the 3rd type of annealing was performed in high-purity oxygen, it was likely that the oxygen-rich atmosphere had better efficiency in removing the residual organics. So, more dye molecules could adsorb onto the TiO_2 nanoparticles, enhancing the transfer of excited electrons from dye to TiO_2 and

Table 3
Photovoltaic performance of the DSSCs assembled with various annealed photoanodes.

Annealing type	Annealing conditions						V_{OC} (volt)	J_{SC} (mA cm^{-2})	FF	η (%)
	1st-step			2nd-step						
1st	Air	450 °C	30 min				0.65	14.08	0.60	5.53
2nd	Air	450 °C	30 min	N_2	300 °C	10 min	0.65	14.83	0.61	5.91
						60 min	0.66	14.89	0.62	6.07
					450 °C	10 min	0.67	15.04	0.67	6.72
						60 min	0.66	15.31	0.67	6.78
3rd	O_2	450 °C	30 min				0.67	15.16	0.57	5.84
4th	O_2	450 °C	30 min	N_2	300 °C	10 min	0.68	14.90	0.59	6.02
						60 min	0.66	14.96	0.63	6.23
					450 °C	10 min	0.65	15.90	0.65	6.70
						60 min	0.66	15.76	0.64	6.70

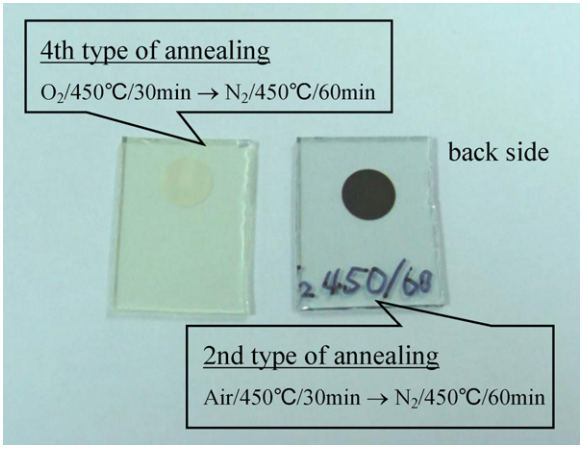

Fig. 4. Appearances of the TiO_2 films after 2nd and 4th types of annealing.

thus promoting J_{SC}. The effects of oxygen-containing atmosphere on removal of the residual organics were discussed in more details in the next section.

When the photoanodes were treated by the 4th type of annealing, the efficiencies of the resultant DSSCs were enhanced over those based on 3rd type of annealing, indicating that additional annealing in nitrogen was beneficial for improvement of the cell performance. As discussed for the 2nd type of annealing, additional annealing in nitrogen could reduce the sheet resistance of ITO and thus enhanced the FF and efficiency of DSSC. It was also found that in the 2nd-step of nitrogen annealing the annealing temperature played a more influential role than the annealing time in the cell performance. Annealing at higher temperature, 450 °C, led to better performance but long term annealing had no significant contribution. This could be explained by the fact that more oxygen vacancies were released due to significant out-diffusion of oxygen atoms from the ITO at higher temperature, reducing the sheet resistance of ITO and thus improving the cell performance. Overall, based on the data shown in Table 3, the 2nd-step annealing in nitrogen was suggested to perform at 450 °C for 10 min.

3.5. *Effect of annealing treatments on removal of residual organics from the TiO_2 films*

As discussed above, annealing in oxygen is likely to be an effective method in removing the residual organics from the TiO_2 film rather than annealing in air. In other words, conventional air annealing might be unable to completely remove the residual organics. This result was consistent with the report from Lee and Kim [11]. To solve this problem, Lee and Kim performed UV-O_3 treatment of the TiO_2 film before and/or after conventional air annealing. Enhanced efficiency of DSSC was observed and the enhancement was attributed to more effective removal of residual organics. In their study, XPS analysis was employed to examine the effects of UV-O_3 treatment on organic removal. In this present study, replacement of air annealing by oxygen annealing was also found to be an effective method in removing the residual organics. Further evidence could be found in Fig. 4, where shows the appearances of the TiO_2-coated ITO substrates after annealing and the annealing conditions thereof. The TiO_2 film on the ITO substrate at the right-hand side changed the color from original white to deep-brown after annealing. It had to point out that the color change was not definitely observed. In all TiO_2-coated ITO substrates tested in this present study, about 40% of samples after the 2nd type of annealing were observed to change the color. Some samples exhibited very significant color change like deep-brown color as seen in Fig. 4, while some exhibited moderate even slight color change. This might be related to some uncertainties resulted from the process variables, for example, the ambient for the TiO_2 screen-printing and that of air annealing. Both might affect the amount of residual organics within the TiO_2 film, thus influence the efficiency of organic removal. For the rest 60% of samples after the 2nd type of annealing, we did not observe any significant color change of the TiO_2-based photoanodes, and the photovoltaic performance of the DSSCs based on these TiO_2-based photoanodes was collected in Table 3 for comparison.

The color change indicated that there were still organic substances remaining in the TiO_2 film after annealing in air and being carbonized after annealing in nitrogen. The DSSC assembled with this deteriorated TiO_2-based photoanode exhibited relatively low efficiency (1–2%). The carbonized organic substances might not only degrade the adsorption of dye molecules onto the TiO_2 nanoparticles but also act as a barrier which hindered transfer of excited electrons from dye molecules to TiO_2. The carbonized organic substances might also reduce light absorption of dye molecules. The above three possibilities could result in the reduction of J_{SC} and thus degraded the cell efficiency.

For all of the test samples after the 4th type of annealing, no significant color change of the TiO_2 films was observed. All of the TiO_2 films still exhibited original white as shown in the sample located at the left-hand side in Fig. 4, suggesting that the 1st-step oxygen annealing had removed majority of the residual organics. Based on the above results, we can conclude statistically that oxygen annealing is a more effective method to remove the residual organics from the TiO_2 film compared with air annealing. Overall, the 4th type of annealing process had two effects. First, more effective adsorption of dye molecules onto the TiO_2 nanoparticles could be achieved by more effective removal of residual organics from the TiO_2 film via the 1st-step of annealing in oxygen. Second, oxygen vacancies in the ITO film increased after the 2nd-step of annealing in nitrogen, reducing the sheet resistance of the ITO film. The above two effects could reduce the internal resistance of cell and enhance the FF and J_{SC}. Therefore, the cell performance could be enhanced.

The effects of oxygen annealing on the photovoltaic performance of the FTO-based DSSC were also investigated. As seen in Table 4, enhanced cell efficiency was observed as the conventional air annealing was replaced by oxygen annealing. FTO is highly thermal resistive and thus its sheet resistance is almost unchanged after annealing. As a result, the FFs of the two types of DSSCs were very close to each other no matter the annealing processes were conducted in air or oxygen. Therefore, the improved cell efficiency was attributed to the enhanced J_{SC} which was the result of the effective removal of residual organics. In addition, it was found that the above FTO-based DSSCs exhibited higher efficiency compared with all of the ITO-based DSSCs prepared in this present study. This may be attributed to the hazy surface of the FTO glass. Commercial FTO glass has a rough surface which can enhance the light scattering on its surface and thereby increases the light harvesting in the TiO_2 layer. Therefore, higher cell efficiency can be obtained.

3.6. *Dependence of fill factor on sheet resistance of ITO substrates*

Fig. 5 shows the fill factors of the DSSCs assembled with various annealed photoanodes. The sheet resistances of the corresponding ITO substrates were also shown for comparison. Clearly, reducing the sheet resistances can enhance the fill factor. In general, fill factor strongly depends upon the internal resistance of the cells. For the DSSCs assembled in this present study, the principal variable that can affect the internal resistance of the cell was the sheet resistance of ITO substrates because the sheet resistance of ITO substrates varied with the annealing conditions as shown in Table 1. Upon reduction of the sheet resistance of ITO substrates, the internal resistance of the cells reduced and thus the fill factors increased.

Table 4
Photovoltaic performance of the DSSCs assembled with FTO substrates annealed in air and oxygen, respectively.

Annealing condition			V_{OC} (volt)	J_{SC} (mA cm^{-2})	FF	η (%)
Air	450 °C	30 min	0.69	14.80	0.71	7.20
O_2	450 °C	30 min	0.73	15.48	0.69	7.82

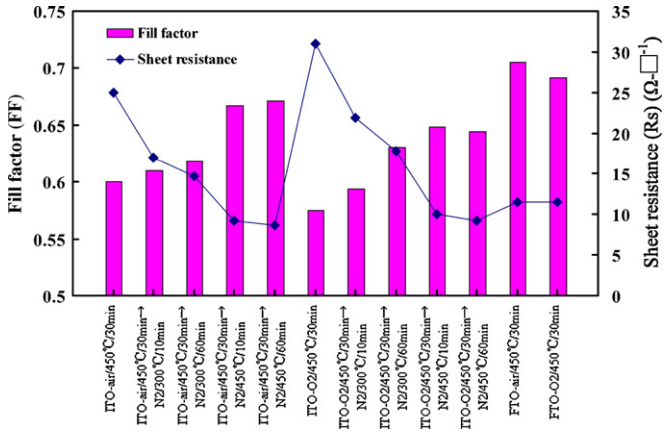

Fig. 5. Fill factors of the DSSCs assembled with various annealed photoanodes. The sheet resistances of the corresponding ITO substrates were also shown for comparison.

4. Conclusions

The conventional one-step air annealing was found to have two detrimental effects on the properties of the photoanode made of TiO_2-coated ITO glass substrate. First, the sheet resistance of ITO increased greatly due to the loss of oxygen vacancies during air annealing. Second, the residual organics within the mesoporous TiO_2 film could not be effectively removed by air annealing. Utilization of two-step annealing treatment, that is, oxygen annealing followed by nitrogen annealing, could significantly enhance the performance of the photoanode as well as the resultant DSSC. By means of 1st-step of annealing in oxygen (450 °C for 30 min), the residual organics were removed more effectively, which enhanced adsorption of dye molecules on the TiO_2 surface and raised the J_{SC} of DSSC. The following 2nd-step of annealing in nitrogen (450 °C for 10 min) effectively removed the extra oxygen atoms incorporated into the ITO film during the 1st-step of annealing in oxygen and released more oxygen vacancies, which reduced the increased sheet resistance of ITO and raised the FF of DSSC. With the enhancement in both J_{SC} and FF, the AM1.5 solar to electric conversion efficiency of DSSC reached 6.7% which is better than that based on the conventional one-step air annealing (5.53%).

Acknowledgements

The authors would like to thank Professor W.P. Dow, Department of Chemical Engineering, National Chung Hsing University, for his help with the UV–vis spectrometer. The work was financially supported by the Ministry of Economic Affairs, Taiwan, ROC. This work is supported in part by the Ministry of Education, Taiwan, ROC under the ATU plan.

References

[1] R.B.H. Tahar, T. Ban, Y. Ohya, Y. Takahashi, J. Appl. Phys. 83 (1998) 2631.
[2] K. Goto, T. Kawashima, N. Tanabe, Sol. Energy Mater. Sol. Cells 90 (2006) 3251.
[3] S. Ngamsinlapasathian, T. Sreethawong, S. Yoshikawa, Thin Solid Films 516 (2008) 7802.
[4] S. Ngamsinlapasathian, T. Sreethawong, Y. Suzuki, S. Yoshikawa, Sol. Energy Mater. Sol. Cells 90 (2006) 2129.
[5] B. Yoo, K. Kim, S.H. Lee, W.M. Kim, N.G. Park, Sol. Energy Mater. Sol. Cells 92 (2008) 873.
[6] Y. Hu, X. Diao, C. Wang, W. Hao, T. Wang, Vacuum 75 (2004) 183.
[7] M.K. Chong, K. Pita, S.T.H. Silalahi, Mater. Chem. Phys. 115 (2009) 154.
[8] E. Burstein, Phys. Rev. 93 (1954) 632.
[9] T.S. Moss, Proc. Phys. Soc. Sect. B 67 (1954) 775.
[10] H. Kim, C.M. Gilmore, A. Piqué, J.S. Horwitz, H. Mattoussi, H. Murata, Z.H. Kafafi, D.B. Chrisey, J. Appl. Phys. 86 (1999) 6451.
[11] B.K. Lee, J.J. Kim, Curr. Appl. Phys. 9 (2009) 404.